Fluid Dynamics and Co-located Conferences
June 24-27, 2013, San Diego, CA
21st AIAA Computational Fluid Dynamics Conference

10.2514/6.2013-2861



# A Time-Spectral Hybridizable Discontinuous Galerkin Method for Periodic Flow Problems

Hemant K. Chaurasia*, Ngoc-Cuong Nguyen† and Jaime Peraire‡
*Massachusetts Institute of Technology, Cambridge, MA 02139, USA*

**We present a Time-Spectral Hybridizable Discontinuous Galerkin (HDG) method for the solution of time-periodic flow problems. Our method combines the Time-Spectral method[1] with a high-order HDG discretization[2,3] in space to achieve the dual benefits of spectral accuracy in time and high-order accuracy in space. Low numerical dissipation is inherited from the HDG method, together with a reduced number of globally coupled degrees of freedom compared to other DG methods. The Time-Spectral method solves the entire time-periodic solution simultaneously, thereby avoiding the cost of resolving undesired initial transient behavior. In contrast to other frequency-domain approaches, the Time-Spectral method represents $(N-1)/2$ Fourier modes by $N$ discrete solution snapshots in time, allowing re-use of many parts of a conventional time-marching code. Convergence properties of the method are demonstrated through applications to periodic convection problems and compressible Navier-Stokes flow over a 2D pitching airfoil. In the latter example, we find that $N = 23$ snapshots are sufficient to predict airfoil loading with the same accuracy as 600 timesteps of a 2-stage $2^{\text{nd}}$-order Diagonally Implicit Runge-Kutta time-marching scheme.**



## I. Introduction

PERIODIC flow problems arise in a broad range of applications, including unsteady aerodynamic analysis of turbomachinery, helicopter rotors, wind turbines and flapping wings. A common approach to computing these flows is to start with a prescribed initial condition and use Runge-Kutta or other time-marching methods to advance a time-accurate solution.[4–6] This approach often requires hundreds of timesteps per period for an acceptable level of time accuracy, and several periods of time-integration before undesired initial transient behavior subsides to reveal the periodic flow solution.

By contrast, a Fourier representation in time can be exploited to compute the same periodic flow state much more efficiently, requiring only a small number of Fourier modes. Reviews of a broad spectrum of such methods are provided by Ekici & Hall,[7] He[8] and Hall *et al.*[9] The first frequency domain methods were the time-linearized methods for small disturbance flows,[10–14] followed by the nonlinear harmonic method for approximately solving large disturbance harmonic flows.[15] A more general method was introduced by Hall *et al.*[16–18] for the computation of large-amplitude unsteady periodic turbomachinery flows. Their Harmonic Balance method was formulated in the frequency domain and involved the solution of spatially-varying mode coefficients. Gopinath & Jameson[1] adapted this method into a new type of Time-Spectral formulation, in which the Fourier representation of the solution was expressed in terms of discrete "snapshots" in the time domain (solution states at discrete time values). This transformation of the Fourier series into the time domain results in a linear system where all snapshots of a certain spatial degree of freedom are coupled to one another. Such a time domain formulation has the advantage that many parts of a conventional time-marching code can be re-used in the implementation of a Time-Spectral solver.

Gopinath & Jameson successfully applied their Time-Spectral method to periodic flow problems such as flapping wings,[1] periodic unsteady vortex shedding,[19] and turbomachinery flows.[20] Their approach employed a low-order Finite Volume spatial discretization. However, in recent years there has been a growing interest in high-order methods, such as the Discontinuous Galerkin (DG) Finite Element methods. These methods

*PhD Candidate, Department of Aeronautics and Astronautics, M.I.T., hemantc@mit.edu, AIAA Student Member.
†Research Scientist, Department of Aeronautics and Astronautics, M.I.T., cuongng@mit.edu, AIAA Member.
‡H.N. Slater Professor of Aeronautics and Astronautics, M.I.T., peraire@mit.edu, AIAA Fellow.

offer greater spatial accuracy and low numerical dissipation, obtained efficiently and with desirable numerical stability properties. In particular, a new class of Hybridizable Discontinuous Galerkin (HDG) methods has emerged which offers the same high-order accuracy and stability of DG methods, but with a reduced number of globally-coupled degrees of freedom.[2,3,21]

In this paper we present a Time-Spectral Hybridizable Discontinuous Galerkin (HDG) method, inheriting the high-order accuracy and low numerical dissipation of the HDG method. One difficulty of many DG methods is the large number of degrees of freedom they employ, due to duplicated degrees of freedom at element interfaces. Constructing a Time-Spectral DG method by coupling several snapshots in time would make for a very expensive algorithm. However, this difficulty is partly mitigated by the special structure of the HDG spatial discretization, which features a substantially reduced number of globally-coupled degrees of freedom while still retaining the high-order accuracy and stability of DG methods. Combining these properties of HDG with the spectral accuracy of a Fourier representation in time, the Time-Spectral HDG method shows promise for delivering high-order accurate solutions to periodic flow problems in a computationally efficient manner.

The sections that follow describe further details of our Time-Spectral HDG method, and examine its performance when applied to both linear convection problems and nonlinear compressible Navier-Stokes flow over a pitching airfoil. Finally, we present some conclusions about the method and directions for future work.



## II. Methodology

### A. Time-Spectral Method

In this section we briefly review the formulation of this Time-Spectral method of Gopinath & Jameson,[1] as it applies to the discretization of the time derivative. In general, a conservation law can be written in semi-discrete form as follows:

$$M\frac{\partial u}{\partial t} + R(u) = 0, \tag{1}$$

where $u$ is the solution vector, $M$ represents a mass matrix, $t$ is time and $R(u)$ is a nonlinear residual vector that is a function of $u$. The discrete Fourier transform of $u$ for a given time period $T$ is:

$$\hat{u}_k = \frac{1}{N}\sum_{n=0}^{N-1} u^n e^{-ikn\frac{2\pi}{T}\Delta t}, \quad k = 1, \ldots, N, \tag{2}$$

where $u^n = u(t^n), 1 \leq n \leq N$, with $t^n = n\frac{2\pi\Delta t}{T}$ and $N$ is the number of snapshots. And its inverse transform is:

$$u^n = \sum_{k=-\frac{N}{2}}^{\frac{N}{2}-1} \hat{u}_k e^{ikn\frac{2\pi}{T}\Delta t}. \tag{3}$$

Therefore, if $\hat{u}_k$ are known then we can recover $u^n$, and vice versa.

Now, from differentiating Equation 3, the discrete time derivative operator can be expressed in terms of frequency domain quantities as:

$$D_t u^n = \frac{2\pi}{T}\sum_{k=-\frac{N}{2}}^{\frac{N}{2}-1} ik\hat{u}_k e^{ikn\frac{2\pi}{T}\Delta t}. \tag{4}$$

This can be rewritten in terms of time domain quantities as:

$$D_t u^n = \sum_{j=0}^{N-1} d_n^j u^j, \tag{5}$$

where $d_n^j$ are constant coefficients which couple all snapshots in time, $u^j$, for each given spatial degree of freedom. For odd $N$, these coefficients are defined:[19]

$$d_n^j = \frac{\pi}{T}(-1)^{n-j}\mathrm{cosec}\left(\frac{\pi(n-j)}{N}\right). \tag{6}$$

Together, Equations 5 & 6 define a Time-Spectral discretization of the time derivative, which can be applied to the semi-discrete form of the governing equation (1). This discretization couples all snapshots of each spatial degree of freedom, requiring that the entire periodic flow solution be solved simultaneously.

### B. Hybridizable Discontinuous Galerkin Method

In the present work we employ a high-order Hybridizable Discontinuous Galerkin (HDG) spatial discretization,[2,3] in contrast to the Finite Volume methods employed in earlier Time-Spectral method work by Gopinath & Jameson.[1] In this section we provide a brief review of the formulation of the HDG method. To this end, we consider the time-dependent convection-diffusion model written as a system of first-order equations

$$\begin{aligned} \boldsymbol{q} + \kappa \nabla u &= 0, && \text{in } \Omega \times (0,T], \\ \frac{\partial u}{\partial t} + \nabla \cdot (\boldsymbol{c} u + \boldsymbol{q}) &= f, && \text{in } \Omega \times (0,T], \\ u &= g_D, && \text{on } \Gamma_D \times (0,T], \\ (\boldsymbol{q} + \boldsymbol{c} u) \cdot \boldsymbol{n} &= g_N, && \text{on } \Gamma_N \times (0,T], \\ u &= u_0, && \text{in } \Omega \text{ for } t = 0. \end{aligned} \tag{7}$$

Here $\Omega \in \mathbb{R}^d$ is the physical domain with boundary $\partial\Omega$, $f \in L^2(\Omega)$ is a source term, $\kappa \in L^\infty(\Omega)$ is a positive diffusivity coefficient, and $\boldsymbol{c} \in (L^\infty(\Omega))^d$ is a smooth velocity vector field.

Let $\mathcal{T}_h$ be a collection of disjoint elements that partition $\Omega$. We denote by $\partial\mathcal{T}_h$ the set $\{\partial K : K \in \mathcal{T}_h\}$. For an element $K$ of the collection $\mathcal{T}_h$, $e = \partial K \cap \partial\Omega$ is the boundary face if the $d-1$ Lebesgue measure of $e$ is nonzero. For two elements $K^+$ and $K^-$ of the collection $\mathcal{T}_h$, $e = \partial K^+ \cap \partial K^-$ is the interior face between $K^+$ and $K^-$ if the $d-1$ Lebesgue measure of $e$ is nonzero. Let $\mathcal{E}_h^o$ and $\mathcal{E}_h^\partial$ denote the set of interior and boundary faces, respectively. We denote by $\mathcal{E}_h$ the union of $\mathcal{E}_h^o$ and $\mathcal{E}_h^\partial$.

Let $\mathcal{P}^p(D)$ denote the set of polynomials of degree at most $p$ on a domain $D$. For any element $K$ of the collection $\mathcal{T}_h$ we denote $W^p(K) \equiv \mathcal{P}^p(K)$ and $\boldsymbol{V}^p(K) \equiv (\mathcal{P}^p(K))^d$. We introduce discontinuous finite element spaces

$$\begin{aligned} W_h^p &= \{w \in L^2(\Omega) \ : \ w|_K \in W^p(K) \ \forall K \in \mathcal{T}_h\}, \\ \boldsymbol{V}_h^p &= \{\boldsymbol{v} \in (L^2(\Omega))^d \ : \ \boldsymbol{v}|_K \in \boldsymbol{V}^p(K) \ \forall K \in \mathcal{T}_h\}. \end{aligned}$$

Here $L^2(D)$ is the space of square integrable functions on $D$. In addition, we introduce a traced finite element space

$$M_h^p = \{\mu \in L^2(\mathcal{E}_h) \ : \ \mu|_e \in \mathcal{P}^p(e), \forall e \in \mathcal{E}_h\}.$$

We also set $M_h^p(g_D) = \{\mu \in M_h^p \ : \ \mu = \mathsf{P} g_D \text{ on } \Gamma_D\}$, where $\mathsf{P}$ denotes the $L^2$-projection into the space $\{\mu|_{\partial\Omega} \ \forall \mu \in M_h^p\}$. Note that $M_h^p$ consists of functions which are continuous inside the faces (or edges) $e \in \mathcal{E}_h$ and discontinuous at their borders.

For functions $\boldsymbol{w}$ and $\boldsymbol{v}$ in $(L^2(D))^d$, we denote $(\boldsymbol{w}, \boldsymbol{v})_D = \int_D \boldsymbol{w} \cdot \boldsymbol{v}$. For functions $u$ and $v$ in $L^2(D)$, we denote $(u, v)_D = \int_D uv$ if $D$ is a domain in $\mathbb{R}^d$ and $\langle u, v \rangle_D = \int_D uv$ if $D$ is a domain in $\mathbb{R}^{d-1}$. We finally introduce

$$(w, v)_{\mathcal{T}_h} = \sum_{K \in \mathcal{T}_h} (w, v)_K, \quad \langle \zeta, \rho \rangle_{\partial\mathcal{T}_h} = \sum_{K \in \mathcal{T}_h} \langle w, v \rangle_{\partial K}, \quad \langle \mu, \eta \rangle_{\mathcal{E}_h} = \sum_{e \in \mathcal{E}_h} \langle \mu, \eta \rangle_e,$$

for functions $w, v$ defined on $\mathcal{T}_h$, $\zeta, \rho$ defined on $\partial\mathcal{T}_h$, and $\mu, \eta$ defined on $\mathcal{E}_h$.

For simplicity of exposition, we consider the Backward-Euler scheme for the discretization of the time derivative. The HDG method then seeks an approximation $(\boldsymbol{q}_h^k, u_h^k, \lambda_h^k) \in \boldsymbol{V}_h^p \times W_h^p \times M_h^p(g_D)$ such that

$$\begin{aligned} (\kappa^{-1} \boldsymbol{q}_h^k, \boldsymbol{v})_{\mathcal{T}_h} - (u_h^k, \nabla \cdot \boldsymbol{v})_{\mathcal{T}_h} + \left\langle \lambda_h^k, \boldsymbol{v} \cdot \boldsymbol{n} \right\rangle_{\partial\mathcal{T}_h} &= 0, \\ \frac{1}{\Delta t^k} \left(u_h^k, w\right)_{\mathcal{T}_h} - (\boldsymbol{c} u_h^k + \boldsymbol{q}_h^k, \nabla w)_{\mathcal{T}_h} + \left\langle (\widehat{\boldsymbol{c}u}_h^k + \widehat{\boldsymbol{q}}_h^k) \cdot \boldsymbol{n}, w \right\rangle_{\partial\mathcal{T}_h} &= (f, w)_{\mathcal{T}_h} + \frac{1}{\Delta t^k} \left(u_h^{k-1}, w\right)_{\mathcal{T}_h}, \\ \left\langle (\widehat{\boldsymbol{c}u}_h^k + \widehat{\boldsymbol{q}}_h^k) \cdot \boldsymbol{n}, \mu \right\rangle_{\mathcal{T}_h} &= \langle g_N, \mu \rangle_{\Gamma_N}, \end{aligned} \tag{8}$$

for all $(\boldsymbol{v}, w, \mu) \in \boldsymbol{V}_h^p \times W_h^p \times M_h^p(0)$, where

$$\widehat{\boldsymbol{c}u}_h^k + \widehat{\boldsymbol{q}}_h^k = \boldsymbol{c}\, \widehat{u}_h^k + \boldsymbol{q}_h^k + \tau(u_h^k - \lambda_h^k)\boldsymbol{n}, \quad \text{on } \partial K.$$

Here we denote $u_h^k = u_h(t^k)$ and $\boldsymbol{q}_h^k = \boldsymbol{q}_h(t^k)$, and $u_h^0$ as the $L^2$ projection of $u_0$ into $W_h^p$. Note that $\tau$ is the so-called stabilization parameter chosen as $\tau = \|\boldsymbol{c}\cdot\boldsymbol{n}\| + \kappa/\ell$ for some characteristic length scale $\ell$.

Other implicit time-stepping methods such as higher-order BDF methods and the fully implicit Runge-Kutta methods can also be used to discretize the time derivative.

### C. Time-Spectral HDG Method

By application of the Time-Spectral method to the PDE system (7), we obtain the following system of equations

$$\begin{aligned} \boldsymbol{Q} + \kappa\nabla\boldsymbol{u} &= 0, \quad \text{in } \Omega\times(0,T], \\ \boldsymbol{D}\boldsymbol{u} + \nabla\cdot\boldsymbol{F}(\boldsymbol{u},\boldsymbol{Q}) &= \boldsymbol{f}, \quad \text{in } \Omega\times(0,T], \end{aligned} \tag{9}$$

where the vector $\boldsymbol{u} = [u^1,\ldots,u^N]^T$ contains $N$ snapshots of the solution over the period $[0,T]$, $\boldsymbol{Q} = [\boldsymbol{q}^1,\ldots,\boldsymbol{q}^N]^T$ with $\boldsymbol{q}^n = \kappa\nabla\boldsymbol{u}^n, n = 1,\ldots,N$, and $\boldsymbol{F}(\boldsymbol{u},\boldsymbol{Q}) = [\boldsymbol{c}u_1 + \boldsymbol{q}_1,\ldots,\boldsymbol{c}u_N + \boldsymbol{q}_N]^T$. Note that $\boldsymbol{D}$ is a square matrix with entries $D_{ij} = d_i^j, 1 \le i,j \le N,$, where $d_i^j$ is given by (6). (In cases where the initial condition $u_0$ is known *a priori*, it can be prescribed by removing the corresponding equations from the system and replacing the source term $\boldsymbol{f}$ with $\tilde{\boldsymbol{f}} = \boldsymbol{f} - u_0\boldsymbol{d_0}$, where $d_0$ is the 1st column of $\boldsymbol{D}$ excluding the 1st entry.)

To formulate the Time-Spectral HDG method we first introduce discontinuous finite element spaces

$$\begin{aligned} \boldsymbol{W}_h^p &= \{\boldsymbol{w}\in(L^2(\Omega))^N \ : \ \boldsymbol{w}|_K \in (W^p(K))^N \ \forall K\in\mathcal{T}_h\}, \\ \boldsymbol{Q}_h^p &= \{\boldsymbol{v}\in(L^2(\Omega))^{N\times d} \ : \ \boldsymbol{v}|_K \in (\boldsymbol{V}^p(K))^N \ \forall K\in\mathcal{T}_h\}, \\ \boldsymbol{M}_h^p &= \{\boldsymbol{\mu}\in(L^2(\mathcal{E}_h))^N \ : \ \boldsymbol{\mu}|_e \in (\mathcal{P}^p(e))^N, \forall e\in\mathcal{E}_h\}. \end{aligned}$$

We set $\boldsymbol{M}_h^p(\boldsymbol{g}_D) = \{\boldsymbol{\mu}\in\boldsymbol{M}_h^p : \boldsymbol{\mu} = \mathsf{P}\boldsymbol{g}_D \text{ on } \Gamma_D\}$. The Time-Spectral HDG method then seeks an approximation $(\boldsymbol{Q}_h,\boldsymbol{u}_h,\boldsymbol{\lambda}_h)\in\boldsymbol{Q}_h^p\times\boldsymbol{W}_h^p\times\boldsymbol{M}_h^p(\boldsymbol{g}_D)$ such that

$$\begin{aligned} (\kappa^{-1}\boldsymbol{Q}_h,\boldsymbol{V})_{\mathcal{T}_h} - (\boldsymbol{u}_h,\nabla\cdot\boldsymbol{V})_{\mathcal{T}_h} + \langle\boldsymbol{\lambda}_h,\boldsymbol{V}\cdot\boldsymbol{n}\rangle_{\partial\mathcal{T}_h} &= 0, \\ (\boldsymbol{D}\boldsymbol{u}_h,\boldsymbol{w})_{\mathcal{T}_h} - (\boldsymbol{F}(\boldsymbol{u}_h,\boldsymbol{Q}_h),\nabla\boldsymbol{w})_{\mathcal{T}_h} + \left\langle\widehat{\boldsymbol{F}}(\boldsymbol{u}_h,\boldsymbol{Q}_h,\boldsymbol{\lambda}_h)\cdot\boldsymbol{n},\boldsymbol{w}\right\rangle_{\partial\mathcal{T}_h} &= (\boldsymbol{f},\boldsymbol{w})_{\mathcal{T}_h} \\ \left\langle\widehat{\boldsymbol{F}}(\boldsymbol{u}_h,\boldsymbol{Q}_h,\boldsymbol{\lambda}_h)\cdot\boldsymbol{n},\boldsymbol{\mu}\right\rangle_{\mathcal{T}_h} &= \langle\boldsymbol{g}_N,\mu\rangle_{\Gamma_N}, \end{aligned} \tag{10}$$

for all $(\boldsymbol{V},\boldsymbol{w},\boldsymbol{\mu})\in\boldsymbol{Q}_h^p\times\boldsymbol{W}_h^p\times\boldsymbol{M}_h^p(0)$, where

$$\widehat{\boldsymbol{F}}(\boldsymbol{u}_h,\boldsymbol{Q}_h,\boldsymbol{\lambda}_h)\cdot\boldsymbol{n} = \boldsymbol{F}(\boldsymbol{u}_h,\boldsymbol{Q}_h)\cdot\boldsymbol{n} + \tau(\boldsymbol{u}_h - \boldsymbol{\lambda}_h), \quad \text{on } \partial K.$$

Of course, the Time-Spectral HDG method will yield a linear system which is several times larger than the linear system of the BDF-HDG method. However, we need to solve the linear system of the Time-Spectral HDG method only once to obtain the numerical solution over the whole time span $[0,T]$. In this paper, we use a direct solver to solve the linear system resulting from (10).

Thus far, we have devised the Time-Spectral HDG method for numerically solving the linear convection-diffusion problem (7) with time-periodic solutions. Extension of this method to nonlinear systems of conservation laws such as the Navier-Stokes equations is rather straightforward, and thus omitted here.

## III. Application to a Time-Periodic Convection Problem

### A. Governing Equation

For our first demonstration of the Time-Spectral HDG method, we solve a time-periodic convection problem in one and two dimensions. A prescribed initial condition will be convected through a domain with spatially periodic boundary conditions, such that the solution wraps around and returns to where it began (making the exact solution of this problem periodic in time). The governing equation can be written:

$$\begin{aligned} &\frac{\partial u}{\partial t} + \nabla\cdot(\mathbf{c}u) = 0 \\ &\qquad \text{in } \ \Omega\times(0,T]. \end{aligned} \tag{11}$$

In the one-dimensional case, we choose a convection velocity of $c = 1$ and a unit domain $\Omega = [0,1]$ with periodic boundary conditions on the left and right, such that the temporal period of the solution is $T = 1$.

The initial condition is chosen to be a Gaussian $u(x,0) = \exp[-200(x-0.5)^2)]$. In the two-dimensional case, we choose a convection velocity of $\mathbf{c} = (1,0)$ and a unit square domain $\Omega = [0,1] \times [0,1]$ with periodic boundary conditions on the left and right, such that the temporal period of the solution is $T = 1$. For the initial condition we choose a Gaussian function $u(\mathbf{x},0) = \exp[-200((x-0.5)^2 + (y-0.5)^2))]$. Homogeneous Dirichlet boundary conditions ($u = 0$) are imposed on the top and bottom boundaries of the square domain, and spatially periodic boundary conditions are imposed on the left and right boundaries.

Note that in this time-periodic convection problem, there is a prescribed initial condition ($t = 0$ solution in the periodic cycle). This contrasts to problems such as pitching airfoil flows, where the $t = 0$ solution is not known *a priori*. In cases where an initial condition is known and required to be prescribed, it is necessary to eliminate the $t = 0$ solution snapshot from the Time-Spectral HDG linear system, reducing by one the number of snapshots to be solved and resulting in an augmented source term.

### B. 1D Results

We first present results from the solution of a one-dimensional version of the time-periodic convection problem described above. High order elements with $p = 4$ polynomials were used. Figure 1 shows that we attain the expected exponential convergence of our Time-Spectral method, as measured in the space-time $L^2$-norm of solution error relative to the known exact solution (perfect convection). Further, this result demonstrates the very small number of snapshots required to fully resolve the solution in time, with only $N = 15$ snapshots (7 Fourier modes) required to fully resolve the solution on our finest grid (20 $p = 4$ high-order elements). Note the behavior of the space-time solution error as the grid is refined – this shows that the total accuracy of the solution is limited by the accuracy of the spatial discretization. With our high-order HDG method, grid refinement increases solution accuracy more efficiently than for low-order methods.

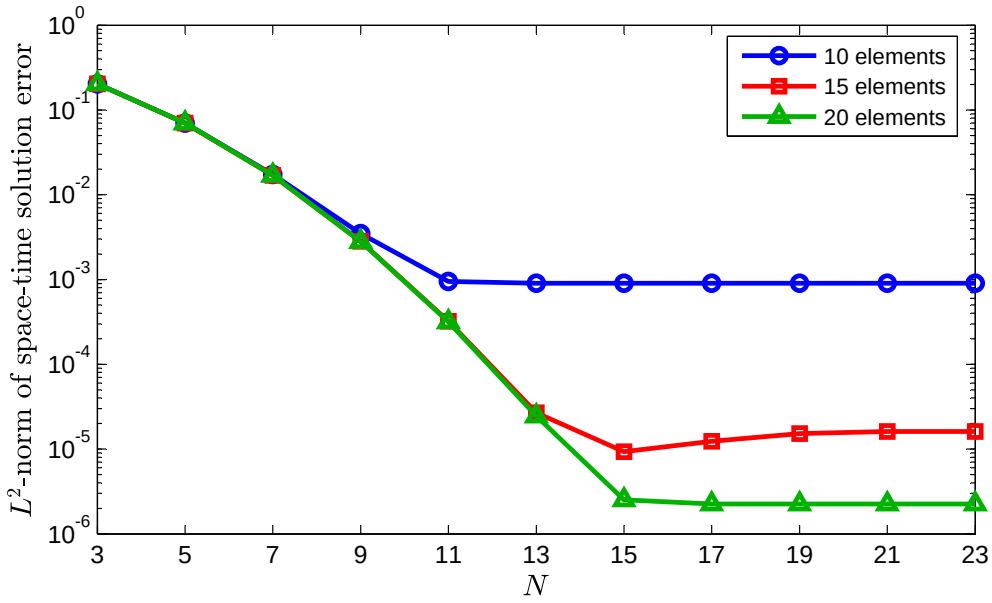


**Figure 1. Convergence of the Time-Spectral HDG method for a 1D time-periodic convection problem, measured by the $L^2$-norm of solution error in both space and time.**

### C. 2D Results

We next present results from the application of our Time-Spectral HDG method to a time-periodic convection problem in two dimensions (as defined in Section A). Figure 2 shows a few representative snapshots of the time-periodic solution, as computed using both implicit time-marching (Backward Euler with 200 timesteps

per period) and our Time-Spectral HDG method (with 21 snapshots, or 10 Fourier modes), on the same spatial grid (128 $p = 3$ high-order elements). These plots visually illustrate the strong numerical dissipation that arises from using low-order implicit timestepping methods without sufficiently small timestep sizes, in contrast to the very high solution accuracy that can be obtained with a much smaller number of Fourier modes by a Time-Spectral method. In this example, 200 timesteps of Backward Euler produced a first-period solution that is visibly much poorer than a Time-Spectral solution with only 21 snapshots.

Figure 3 quantifies the convergence properties of our Time-Spectral HDG method in this 2D convection application, showing that we attain the expected exponential convergence in the space-time $L^2$ error norm. Here we also show a comparison of the convergence behavior for high-order spatial grids with the same number of elements but different polynomial orders $p$. Increasing $p$ offers a convenient and efficient way to decrease solution error. Here we see the spatial accuracy advantages of the high-order HDG method appearing in combination with the temporal accuracy advantages of the Time-Spectral method.

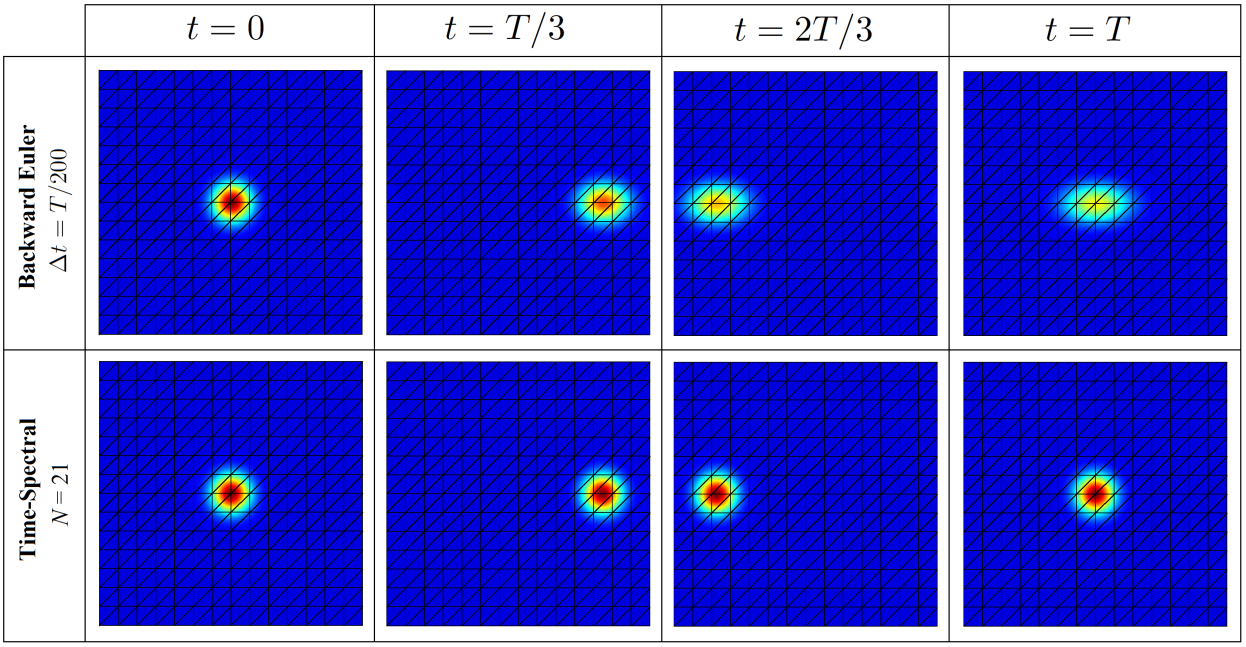


**Figure 2. Solution snapshots for a 2D time-periodic convection problem, contrasting the behavior of implicit Backward Euler time-marching with 200 timesteps per period (*upper plots*) against the present work's Time-Spectral method with only $N = 21$ snapshots (10 harmonic modes) (*lower plots*).**

## IV. Application to a Pitching Airfoil

Here we demonstrate the performance of the Time-Spectral HDG method in a nonlinear setting by solving the periodic flow over a pitching airfoil at $Re = 1000$.

### A. Problem Description

The airfoil has a symmetric NACA 0012 profile, and moves with an oscillatory vertical translation and angle of attack defined by:

$$y(t) = A\cos(2\pi t/T), \qquad \alpha(t) = B\sin(2\pi t/T). \tag{12}$$

Constants used in this example are: period $T = 5$, heaving amplitude $A = 0.125$, and pitch amplitude $B = 5°$. These parameters correspond to a Strouhal number of $St = 0.05$. The Reynolds number of the flow is $Re = 1000$ and the inflow Mach number is $M_\infty = 0.2$. The governing equations for this problem are the laminar compressible Navier-Stokes equations, incorporating an Arbitrary Lagrangian-Eulerian (ALE)[6] formulation to account for mesh motion. The computational domain is discretized by a high-order C-mesh with 560 elements, shown in Figure 4.

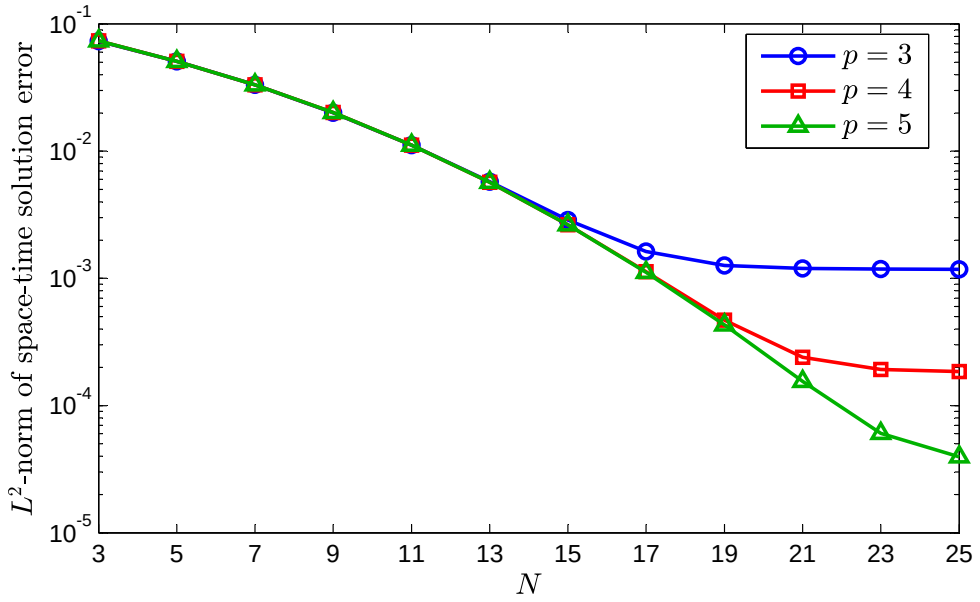


**Figure 3. Convergence of the Time-Spectral HDG method for 2D time-periodic convection problem, measured by the $L^2$-norm of solution error in both space and time.**

## B. Computational Results

Flow around a pitching airfoil was solved using the Time-Spectral HDG method with several different numbers of snapshots $N$, and on meshes with three different spatial orders ($p = 3, 4, 5$). To assess the accuracy of the Time-Spectral HDG method in time, solutions were also obtained using an HDG method with a Diagonally Implicit Runge-Kutta (DIRK) time-marching scheme.[22,23] Time-marched solutions obtained by a 3-stage, 3$^{\text{rd}}$-order DIRK scheme with a very small timestep size ($\Delta t = T/200$) were used as "truth" solutions for comparison with the Time-Spectral results.

Several interesting observations follow from the results of these computations. First of all, Figure 5 illustrates the effects of initial transient flow behavior on time-marched and Time-Spectral solutions. Shown here through the lift coefficient time-series, a fully resolved DIRK(3,3) time-marched solution undergoes an initial transient flow behavior that takes at least 3 full oscillation periods to subside. This behavior is not due to numerical inaccuracy – rather, it is the physical behavior of the flow following the necessarily imperfect initial condition prescribed for the flow at the beginning of time-marching. The result is that 3 full periods of time-integration (300 or 600 timesteps in the example shown) are required before the computed flow can reach a repeating periodic state. In contrast, the fully resolved Time-Spectral solution shown in this figure completely avoids the initial transient behavior of the flow. The Time-Spectral method solves the entire periodic flow state simultaneously. The ability to avoid the cost of resolving undesired initial transient behavior is a key advantage of the Time-Spectral method.

The next observation is that the Time-Spectral HDG solution converges very rapidly to a fully time-resolved solution. For example, Figure 6 shows the airfoil lift coefficient time-series computed by the Time-Spectral HDG method with several different numbers of snapshots, $N$. Here we see that with only $N = 5$ snapshots (corresponding to just 2 harmonic modes), the lift coefficient time-series is surprisingly close to the fully resolved solution. With $N = 11$ snapshots it is even closer, and at $N = 21$ snapshots we can no longer see the difference visually.

For another perspective, Figure 7 uses the computed flow-fields to illustrate convergence of the Time-Spectral HDG method. Here we show the flow-field at a few representative snapshots in time, as computed by a Time-Spectral HDG method with $N = 5$ snapshots, a Time-Spectral HDG method with $N = 27$ snapshots, and a highly resolved time-marched HDG solution serving as a "truth" reference (computed using DIRK(3,3)

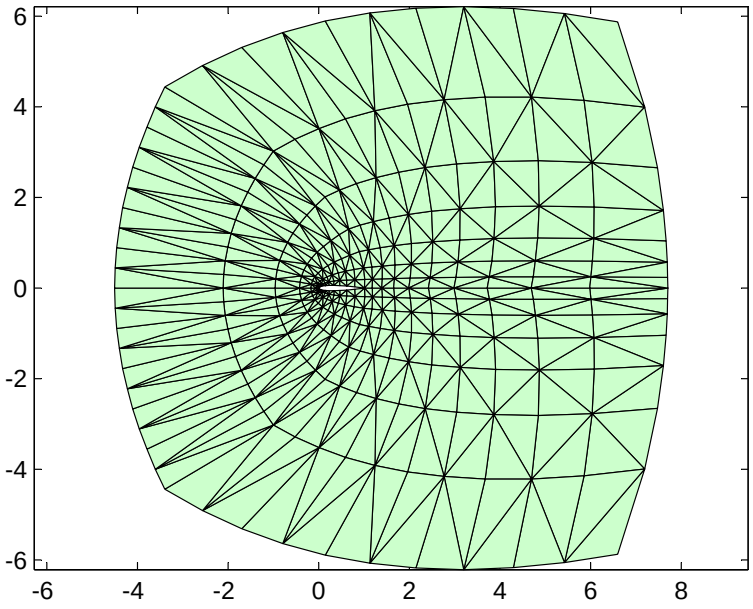


**Figure 4. High-order mesh for pitching airfoil problem.**

with timestep $\Delta t = T/200$ as previously mentioned). The flow-field from the $N = 5$ Time-Spectral solution is clearly underresolved in time, smearing out the wake region of the flow. However, since the flow near the airfoil appears well-resolved, the airfoil lift coefficient (Figure 6) can be predicted more accurately than one might expect. At $N = 27$ snapshots however, the flow is so well resolved that we visually cannot distinguish this flow from the highly resolved time-marched solution on the right.

To quantify the convergence of the Time-Spectral HDG method more precisely, Figure 8 presents the $L^2$-norm of the error in the lift coefficient timeseries across a range of Time-Spectral HDG solutions with different numbers of snapshots $N$ and different spatial orders $p$. For each spatial order $p$, the error norm is computed with respect to a very highly resolved time-marched solution on the same mesh, obtained using the 3-stage, $3^{\text{rd}}$-order DIRK scheme mentioned previously. This plot shows the exponential convergence in $N$ that we expect of the Time-Spectral method, as we observed in the convection problems presented earlier in this paper. The different curves for each spatial order $p$ showcase the high-order accuracy of the HDG method, the ease with which we can obtain a more accurate solution on the same mesh, and the large gains in accuracy that can be achieved at higher $p$.

Finally, we note an interesting point of comparison between the Time-Spectral HDG method and the DIRK time-marched HDG method. A periodic flow solution was obtained for the pitching foil problem using a 2-stage, $2^{\text{nd}}$-order DIRK scheme with $\Delta t = T/100$ over 6 periods on a $p = 5$ high-order mesh. Measuring solution error the same way as in Figure 8, we found the error norm to be 0.0036. Referring the Figure 8, we find that the Time-Spectral HDG solution with $N = 23$ snapshots has an error no greater than the DIRK(2,2) solution. That is, for this demonstration problem, $N = 23$ snapshots are sufficient to predict airfoil loading with the same accuracy as 600 timesteps of a 2-stage $2^{\text{nd}}$-order Diagonally Implicit Runge-Kutta time-marching scheme.

## V. Conclusions & Future Work

In this paper we have presented a Time-Spectral, high-order Hybridizable Discontinuous Galerkin (HDG) method for solving time-periodic flow problems, and have demonstrated the performance of the method on linear convection problems and compressible Navier-Stokes flow over a 2D pitching airfoil. These examples have demonstrated exponential convergence in time with the number of snapshots $N$, and similar performance

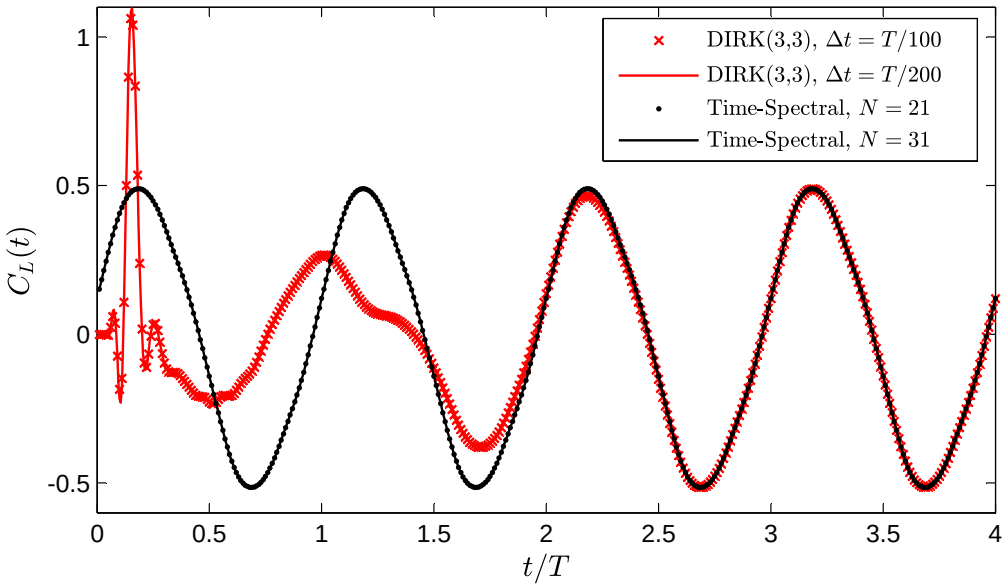


**Figure 5. The effect of undesired initial transient behavior is evident in the lift coefficient $C_L(t)$ computed from a fully resolved DIRK(3,3) time-marched solution (*red*), compared with a fully resolved Time-Spectral solution (*black*). In this case, the time-marched solution must be integrated for 3 full periods (300/600 timesteps) before the initial transient gives way to a periodic flow state.**

can be expected more generally for problems with a smooth variation in time.

Key advantages of the Time-Spectral HDG method for the solution of periodic flow problems include:

- High-order accuracy and low numerical dissipation are inherited from the HDG spatial discretization.
- HDG provides a reduced number of globally coupled degrees of freedom compared to other DG methods, helping to mitigate the difficulties associated with the large size of the Time-Spectral linear system.
- The Time-Spectral discretization provides exponential convergence in the number of snapshots $N$, and for many problems the required number of snapshots $N$ could be very low. (For the pitching airfoil problem presented in this paper, $N = 23$ was sufficient to predict airfoil loading with the same accuracy as a highly resolved DIRK(2,2) solution time-marched over 600 timesteps.)
- The Time-Spectral approach also computes the periodic solution directly, avoiding the cost of resolving undesired initial transient behavior.

A key challenge facing this method is the large size of the associated linear system, with $N$ times more degrees of freedom and a Jacobian matrix $N^2$ times larger than the time-marching case. In favor of the Time-Spectral HDG method, this larger system must only be solved once to obtain the solution over the entire period $[0, T]$. To enable the solution of larger flow problems, further work is now underway to develop an iterative solver for the Time-Spectral HDG system which appropriately exploits the structure of the Time-Spectral time-derivative term. Block Jacobi preconditioning may prove effective, given the larger block size in the Time-Spectral HDG system matrix (dense diagonal blocks are $N^2$ times larger). On the application side, work is in progress to combine the Time-Spectral HDG method with a sliding mesh interface for application to turbomachinery flow problems.

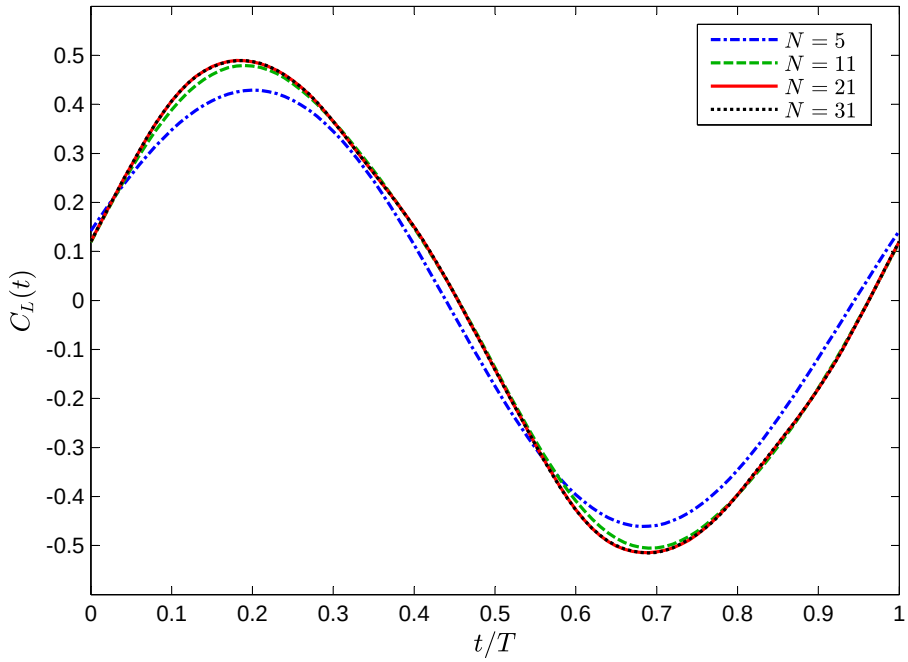


**Figure 6. Rapid convergence of the Time-Spectral HDG solution to the pitching airfoil problem is seen in the lift coefficient $C_L(t)$, shown here for different numbers of snapshots, $N$.**



## Acknowledgments

The authors would like to acknowledge partial financial support for this work from Pratt & Whitney, the Singapore-MIT Alliance and the Air Force Office of Scientific Research under grant FA9550-12-0357. The authors would also like to thank Xevi Roca for helpful discussions and advice during the development of the methods presented here.

## References

[1]Gopinath, A. and Jameson, A., "Time Spectral Method for Periodic Unsteady Computations over Two- and Three-Dimensional Bodies," *43rd Aerospace Sciences Meeting and Exhibit*, Reno, Nevada, January 2005, AIAA Paper 2005-1220.

[2]Nguyen, N.-C., Peraire, J., and Cockburn, B., "An implicit high-order hybridizable discontinuous Galerkin method for linear convection–diffusion equations," *Journal of Computational Physics*, Vol. 228, No. 9, 2009, pp. 3232–3254.

[3]Nguyen, N.-C., Peraire, J., and Cockburn, B., "An implicit high-order hybridizable discontinuous Galerkin method for nonlinear convection-diffusion equations," *J. Comp. Phys.*, Vol. 228, 2009, pp. 8841–8855.

[4]Giles, M., "Calculation of unsteady wake/rotor interaction," *J. Propulsion*, Vol. 4, No. 4, 1988, pp. 356–362.

[5]He, L. and Denton, J., "Three-dimensional time-marching inviscid and viscous solutions for unsteady flows around vibrating blades," *Journal of Turbomachinery*, Vol. 116, 1994, pp. 469–476.

[6]Persson, P.-O., Bonet, J., and Peraire, J., "Discontinuous Galerkin solution of the Navier-Stokes equations on deformable domains," *Computer Methods in Applied Mechanics and Engineering*, Vol. 198, No. 17-20, 2009, pp. 1585 – 1595.

[7]Ekici, K. and Hall, K., "Nonlinear analysis of unsteady flows in multistage turbomachines using harmonic balance," *AIAA Journal*, Vol. 45, 2007, pp. 1047–1057.

[8]He, L., "Fourier methods for turbomachinery applications," *Progress in Aerospace Sciences*, Vol. 46, No. 8, 2010, pp. 329–341.

[9]Hall, K., Ekici, K., Thomas, J., and Dowell, E., "Harmonic balance methods applied to computational fluid dynamics problems," *International Journal of Computational Fluid Dynamics*, , No. ahead-of-print, 2012, pp. 1–16.

[10]Verdon, J., Adamczyk, J., and Caspar, J., "Subsonic flow past an oscillating cascade with steady blade loading – Basic formulation," *Unsteady Aerodynamics, edited by R. B. Kinney, proceedings of a symposium held at the University of Arizona*, Vol. 2, Tucson, Ariz., March 1975, pp. 827–851.

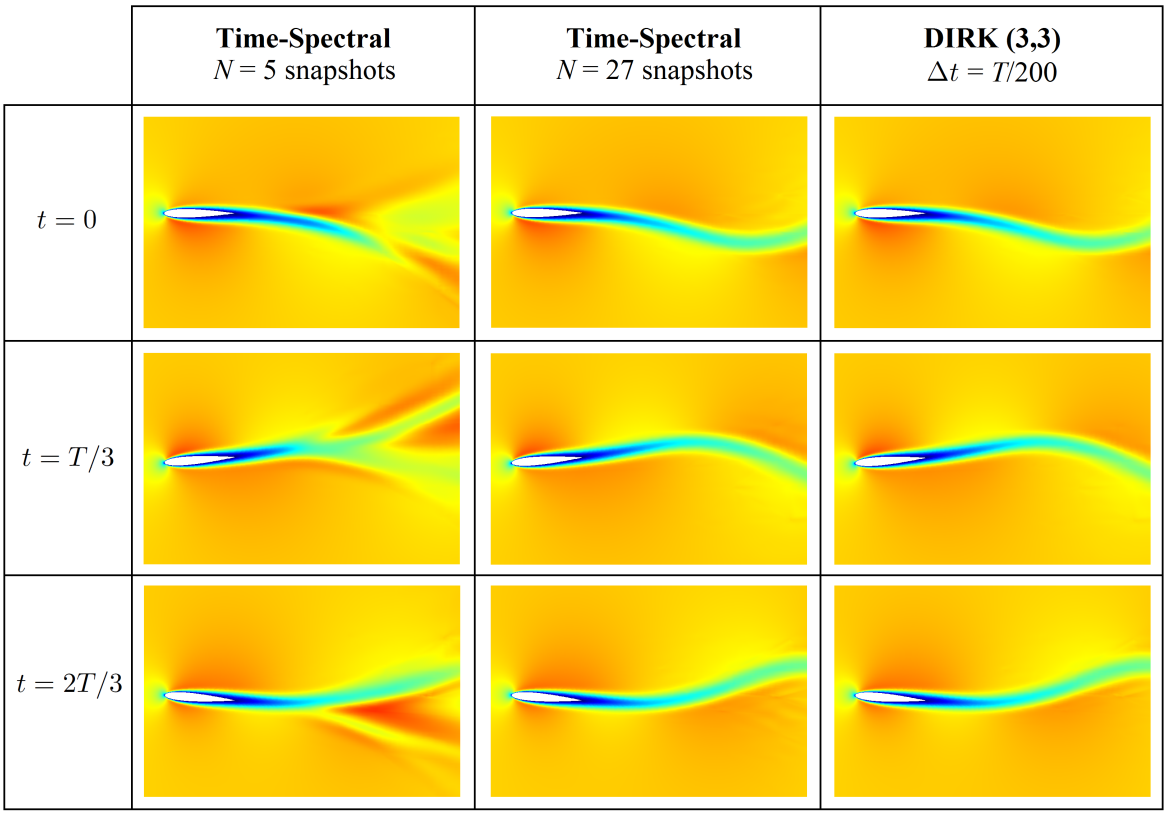


**Figure 7. Snapshots of the periodic flow solution for our pitching airfoil problem, solved by 3 different time discretization schemes: Time-Spectral HDG with $N = 5$ snapshots; Time-Spectral HDG with $N = 27$ snapshots; and a very highly resolved time-marching HDG solution, used as a "truth" reference. The time-marched solution was obtained by a 3-stage, 3rd-order Diagonally Implicit Runge-Kutta (DIRK) scheme with 200 timesteps per period over 6 periods of integration.**



[11]Verdon, J. and Caspar, J., "Subsonic Flow Past an Oscillating Cascade with Finite Mean Flow Deflection," *AIAA Journal*, Vol. 18, No. 5, May 1980, pp. 540–548.

[12]Verdon, J. and Caspar, J., "A linearized unsteady aerodynamic analysis for transonic cascades," *Journal of Fluid Mechanics*, Vol. 149, 1984, pp. 403–429.

[13]Hall, K. and Crawley, E., "Calculation of unsteady flows in turbomachinery using the linearized Euler equations," *AIAA Journal*, Vol. 27, 1989, pp. 777.

[14]Clark, W. and Hall, K., "A time-linearized Navier-Stokes analysis of stall flutter," *Journal of Turbomachinery*, Vol. 122, 2000, pp. 467–476.

[15]He, L. and Ning, W., "Efficient approach for analysis of unsteady viscous flows in turbomachines," *AIAA Journal*, Vol. 36, No. 11, 1998, pp. 2005–2012.

[16]Hall, K., "Computation of unsteady nonlinear flows in cascades using a harmonic balance technique," *Kerrebrock symposium - a symposium in honor of Professor Jack L. Kerrebrocks 70th birthday*, Massachusetts Institute of Technology, Cambridge, MA, 1998.

[17]Hall, K., Thomas, J., and Clark, W., "Computation of Unsteady Nonlinear Flows in Cascades Using a Harmonic Balance Technique," *9th international symposium on unsteady aerodynamics, aeroacoustics and aeroelasticity of turbomachines*, Lyon, France, September 2000.

[18]Hall, K., Thomas, J., and Clark, W., "Computation of Unsteady Nonlinear Flows in Cascades Using a Harmonic Balance Technique," *AIAA Journal*, Vol. 40, No. 5, May 2002, pp. 879–886.

[19]Gopinath, A. and Jameson, A., "Application of the Time Spectral Method to Periodic Unsteady Vortex Shedding," *44th AIAA Aerospace Sciences Meeting and Exhibit*, Reno, Nevada, January 2006, AIAA Paper 2006-0449.

[20]Gopinath, A., *Efficient Fourier-Based Algorithms for Time-Periodic Unsteady Problems*, Ph.D. thesis, Stanford University, 2007.

[21]Nguyen, N.-C., Peraire, J., and Cockburn, B., "Hybridizable discontinuous Galerkin methods," *Spectral and High Order Methods for Partial Differential Equations*, 2011, pp. 63–84.

[22]Alexander, R., "Diagonally Implicit Runge-Kutta Methods for Stiff O.D.E.'s," *SIAM Journal on Numerical Analysis*, Vol. 14, No. 6, 1977, pp. 1006–1021.

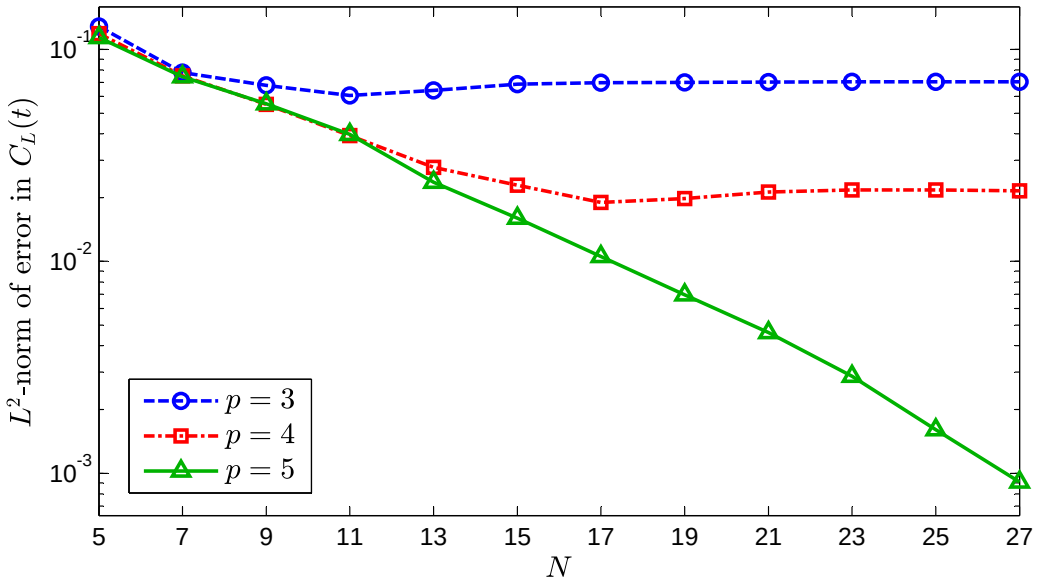


**Figure 8. Spectral convergence of computed airfoil lift coefficient $C_L(t)$ using the Time-Spectral HDG method with an increasing number of snapshots $N$. The 3 curves represent different spatial polynomial orders $p$ on the same grid, highlighting the high-order accuracy of our method. At lower spatial orders ($p$), we see that fewer snapshots $N$ are required to fully resolve the solution in time.**

[23]Peraire, J., Nguyen, N.-C., and Cockburn, B., "A Hybridizable Discontinuous Galerkin Method for the Compressible Euler and Navier-Stokes Equations," *48th AIAA Aerospace Sciences Meeting and Exhibit*, Orlando, FL, January 2010, AIAA paper 2010-363.